CMS Physics Analysis Summary

Contact: cms-pag-conveners-b2g@cern.ch 2014/08/07

Search for pair-produced vector-like quarks of charge $-\frac{1}{3}$ in same-sign dilepton final state

The CMS Collaboration

Abstract

The results of a search for pair-produced vector-like quarks with charge $-\frac{1}{3}$ are presented. The analysis was performed using a dataset of pp collisions at $\sqrt{s} = 8$ TeV collected with the CMS detector and corresponding to an integrated luminosity of 19.6 fb^{-1}. Events with a same-sign lepton pair and hadronic activity are selected and no excess above expected Standard Model backgrounds is observed. The results are used to set limits on the mass of the b′ quark as a function of its branching ratio to tW, bZ and bH. The data excludes a b′ quark with mass less than 800 GeV if the decay is to a top and W exclusively.

1 Introduction

A Higgs boson (H) with the properties predicted by the standard model (SM) was discovered with a mass of 125 GeV at the LHC [1–3]. This mass suggests the need for a mechanism to stabilize any quantum loop corrections in a calculation of this mass, since these corrections diverge quadratically with the cutoff scale of the calculation. Several models that mitigate this divergence involve the introduction of heavy vector-like quarks. For instance, vector-like quarks are predicted in little Higgs [4], composite Higgs [5], and warped extra dimension [6] models. Vector-like quarks have left- and right-handed components under the standard model gauge group and their masses are generated independently from the Higgs boson coupling. They can be pair produced via their gauge coupling to gluons, and decay through the exchange of W, Z, and H bosons. The main decay modes are charged current decays into a top quark and a W boson ($\mathrm{b}' \to \mathrm{tW}$), flavor-changing neutral current(FCNC) decays into a bottom quark with a Z boson ($\mathrm{b}' \to \mathrm{bZ}$), or a bottom quark with a Higgs boson ($\mathrm{b}' \to \mathrm{bH}$) [7]. Several searches for vector-like quarks have been performed by the CMS and ATLAS experiments [8–13]. In this note we search for pair-produced vector-like quarks of charge $-\frac{1}{3}$, denoted by b', based on a data sample recorded by the CMS detector at $\sqrt{s} = 8$ TeV, corresponding to an integrated luminosity of 19.6 fb^{-1}. The b' quarks decay into three different final states, $\mathrm{b}' \to \mathrm{tW}$, bZ, and bH, with the sum of the branching fractions into these three final states equal to unity. Some of the $\mathrm{b}'\overline{\mathrm{b}}'$ decay combinations, for example the decay of $\mathrm{b}'\overline{\mathrm{b}}' \to \mathrm{tW}^-\bar{\mathrm{t}}\mathrm{W}^+$, $\mathrm{tW}^-\overline{\mathrm{b}}\mathrm{H}$, or $\mathrm{bH}\overline{\mathrm{b}}\mathrm{H}$, can produce a final state of $\mathrm{bW}^+\mathrm{W}^-\overline{\mathrm{b}}\mathrm{W}^+\mathrm{W}^-$, which leads to a unique signature of same-sign dileptons and multiple jets, if two W bosons decay leptonically. In this analysis, events are selected that have two isolated leptons with the same electric charge. Such a distinctive signature of same-sign dilepton occurs rarely in the standard model.

2 The CMS detector

The central feature of the Compact Muon Solenoid (CMS) apparatus is a superconducting solenoid of 6 m internal diameter, providing a magnetic field of 3.8 T. Within the superconducting solenoid volume are a silicon pixel and strip tracker, a lead tungstate crystal electromagnetic calorimeter (ECAL), and a brass/scintillator hadron calorimeter (HCAL). Muons are measured in gas-ionization detectors embedded in the steel return yoke outside the solenoid. Extensive forward calorimetry complements the coverage provided by the barrel and endcap detectors. CMS uses a right-handed coordinate system, with the origin at the nominal interaction point, the x axis pointing to the centre of the LHC, the y axis pointing up (perpendicular to the LHC plane), and the z axis along the anticlockwise-beam direction. The polar angle θ is measured from the positive z axis and the azimuthal angle ϕ is measured in the x-y plane. The first level of the CMS trigger system, composed of custom hardware processors, uses information from the calorimeters and muon detectors to select the most interesting events in a fixed time interval of less than 4 μs. The High Level Trigger processor farm further decreases the event rate from around 100 kHz to around 300 Hz, before data storage. A more detailed description can be found in Ref. [14].

3 Selection criteria

We use the particle flow reconstruction algorithm [15]. The particle flow algorithm aims to reconstruct and identify each single particle with an optimized combination of all sub-detector information. Each particle is categorized into five types known as particle-flow candidates:

muons, electrons, photons, charged hadrons, and neutral hadrons. The energy of photons is directly obtained from the ECAL measurement, corrected for zero-suppression effects. The energy of electrons is determined from a combination of the track momentum at the main interaction vertex, the corresponding ECAL cluster energy, and the energy sum of all bremsstrahlung photons attached to the track. The energy of muons is obtained from the corresponding track momentum measured using the silicon tracking system. The energy of charged hadrons is determined from a combination of the track momentum and the corresponding ECAL and HCAL energy, corrected for zero-suppression effects, and calibrated for the nonlinear response of the calorimeters. Finally, the energy of neutral hadrons is obtained from the corresponding calibrated ECAL and HCAL energy.

Electron candidates are reconstructed with a cluster of ECAL energy deposits that match hits in the silicon tracker [16]. Electrons are required to have a minimum transverse momentum of 20 GeV. The electron candidates are required to be within the region of $|\eta| < 2.4$, where the pesudorapidity η is defined by $-\ln[\tan(\theta/2)]$ and θ is the polar angle. The candidates in the transition region between barrel and endcap detectors ($1.44 < |\eta| < 1.57$) are excluded. Electrons are selected using variables that include the ratio of energy deposited in the hadronic and electromagnetic calorimeters, the width of the calorimeter shower in η, and the distance of closest approach of the projected candidate-electron trajectory in the tracker to the axis of electromagnetic shower. The electron track is required to originate from the primary interaction vertex, which is defined by the vertex associated with tracks yielding the largest value for the sum of their p_T^2. The electron candidates which are consistent with originating from photon conversions are rejected.

Muon candidates are reconstructed with a global fit to trajectories, using the hits in the inner tracker and in the muon system. Muons are required to have transverse momenta $p_T > 20$ GeV and pseudorapidities $|\eta| < 2.4$. The muon candidate must be associated with hits in the silicon pixel and strip detectors, and track segments in the muon chambers. The muon reconstruction requires a high-quality global fit to the track segments. The muon track is required to originate from the primary vertex.

Electrons and muons from $W \to \ell\nu$ ($\ell = e, \mu$) decays are expected to be isolated from other physics in the detector. A cone of $\Delta R < 0.3$ (0.4), where $\Delta R \equiv \sqrt{(\Delta\eta)^2 + (\Delta\phi)^2}$, is constructed around each electron-(muon-)candidate's direction. An isolation variable is defined by the scalar sum of the transverse momenta of the particles inside the cone, excluding contributions from the lepton candidate, divided by the p_T of the candidate. If this isolation variable exceeds 15% (12%), then the electron (muon) candidate is rejected. Electron candidates are required to be separated from any selected muon candidates by $\Delta R > 0.1$ to remove misidentified electrons from muon bremsstrahlung. Tau candidates which decay hadronically are reconstructed using the hadron-plus-strips algorithm [17]. If a hadronic tau candidate exists in an event and is within the kinematical region of $p_T > 20$ GeV and $|\eta| < 2.3$, the event is rejected from the analysis.

Jets are reconstructed offline by clustering particle flow candidates using the anti-k_T algorithm [18] with a size parameter of 0.5, using `fastjet` version 3.0 [19]. Jet candidates are required to have $p_T > 30$ GeV and $|\eta| < 2.4$. The jet momentum is determined from the sum of all particle momenta in this jet. The measured jet energies are calibrated to correct the energy response obtained from data and simulations [20]. Neutrinos from W or Z boson decays escape the detector, and thereby give rise to a significant imbalance in the transverse momentum (MET) measured for each event. This MET is defined as the absolute value of the vector sum

of the transverse momenta of all reconstructed particles.

Considering the full decay chain of $pp \to b'\bar{b}' \to tW^+tW^-, tW^+bH, bHbH \to bW^+W^-bW^+W^-$, there are two b-jets and four W bosons. If two W bosons of the same charge decay leptonically, and the other two W bosons decay hadronically, it leads to a complex final state of same-sign lepton pair and 6 jets, where two of the jets are from b-quarks.

Selected events are required to have at least 4 jets. In each event, two lepton candidates of the same electric charge are selected. The lepton candidates can be either two electrons, two muons, or an electron and a muon. If there is an additional electron, muon, or tau candidate, the event is rejected from this analysis.

A full reconstruction of $b'\bar{b}'$ events is not foreseen, thus the variable S_T is defined with the following equation:

$$S_T = \sum p_T(\text{jets}) + \sum p_T(\text{leptons}) + \text{MET}\,, \tag{1}$$

which also provides a good sensitivity to the decay of heavy objects. Events with S_T smaller than 200 GeV and MET < 30 GeV are rejected. The search regions are defined as five S_T bins ($200 \leq S_T < 400$, $400 \leq S_T < 600$, $600 \leq S_T < 800$, $800 \leq S_T < 1200$, and $S_T \geq 1200$) and three channels ($\mu\mu$, ee, and μe).

The simulated signal $pp \to b'\bar{b}'$ events are generated with the MADGRAPH v5.1.3.30 [21] generator, with up to two additional partons from the hard collision. The samples are generated in steps of 50 GeV, ranging from 450 to 1000 GeV, for the mass of the b' quark. Production cross sections of $pp \to b'\bar{b}'$ are estimated up to next-to-next-to-leading-order (NNLO) [22] in α_s. The samples are simulated with the CMS GEANT-based simulation described in [23]. The decay of the the b' quark, parton showering and hadronization are simulated with PYTHIA 6.4.26 [24]. Acceptances of b' signals are estimated for various branching fraction mixtures for each mass point (see Figure 1). The maximum acceptance is found to be 1.90% if the b' quark only decays to a top quark and a W boson; the minimum acceptance is estimated to be 0.001% if the b' quark only decays to a bottom quark and a Z boson.

Table 1: Summary of production cross section of $pp \to b'\bar{b}'$ processes with various assumption of b' quark mass. The cross sections are estimated up to NNLO in α_s.

M(b') [GeV]	Cross section σ [pb]
450	1.153
500	0.590
550	0.315
600	0.174
650	0.0999
700	0.0585
750	0.0350
800	0.0213
850	0.0132
900	0.00828
950	0.00525
1000	0.00336

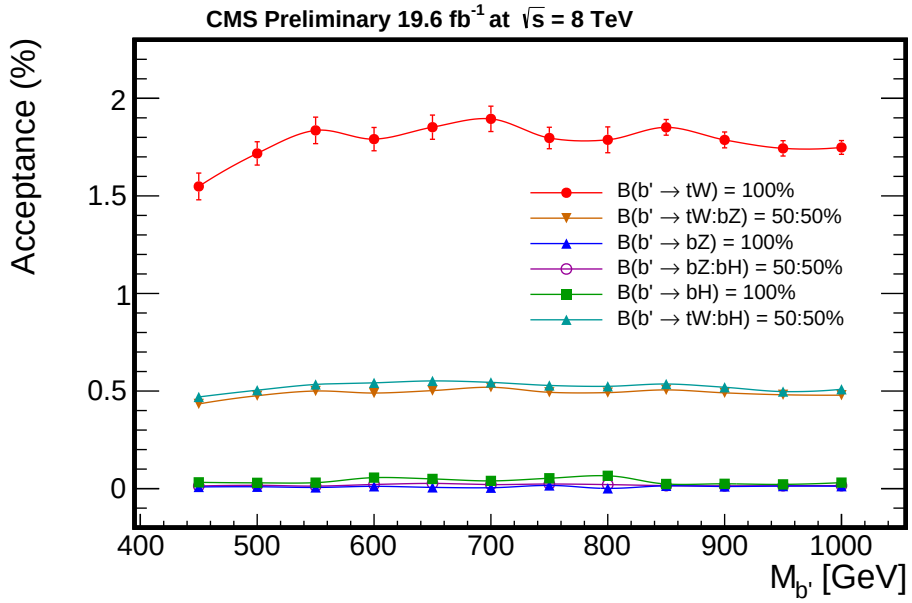

Figure 1: The signal acceptance according to the branching fraction $\mathcal{B}(b' \to tW) = 100\%$, $\mathcal{B}(b' \to tW : bZ) = 50\% : 50\%$, $\mathcal{B}(b' \to bZ) = 100\%$, $\mathcal{B}(b' \to bZ : bH) = 50\% : 50\%$, $\mathcal{B}(b' \to bH) = 100\%$, and $\mathcal{B}(b' \to bH : tW) = 50\% : 50\%$ for each mass point. The maximum acceptance is found to be 1.90% if the b' quark only decays to a top quark and a W boson; the minimum acceptance is estimated to be 0.001% if the b' quark only decays to a bottom quark and a Z boson.

4 Background estimation

Backgrounds are categorized into four types: (i) events with two prompt leptons of the same charge; (ii) prompt $\ell^+\ell^-$ events with an electron that has a misidentified charge; (iii) single prompt lepton events with a non-prompt lepton that has been misidentified as prompt; and (iv) events with two non-prompt leptons.

The first category with two prompt leptons of the same charge is irreducible, but it is very rare in the standard model, including $pp \to ttW, ttZ$, diboson, and triboson processes. The contribution from this source is estimated with the simulated samples.

The second category is formed using charge-misidentified electron candidates. The charge-misidentification rate is measured using a combination of $Z + jets$ and $t\bar{t} + jets$ processes from the ratio of same-sign dilepton events to opposite-sign dilepton events. The background contribution in the signal region is estimated by multiplying the charge-misidentified rate by the number of events in a charge-misidentification control region, which is defined with identical selection criteria as the signal region, except selecting the opposite-sign dilepton events.

A "Tight-to-Loose" (T/L) method is introduced to estimate the remaining backgrounds. The "tight" leptons pass the selection defined above. The "loose" muon candidates have to pass a relaxed isolation threshold, a relaxed requirement on the impact parameters, and a relaxed track-fit quality threshold. The "loose" electron candidates have to pass a relaxed identification criteria and a relaxed isolation threshold. Tight lepton candidates are excluded from the loose lepton candidates. Several control regions are defined by replacing one or two "tight" leptons with "loose" leptons. The numbers of events in these control regions are labeled as N_{TT}, N_{TL},

N_{LT}, and N_{LL}, where the subscripts T and L denote the "tight" lepton and "loose" lepton, respectively.

The yields for the background events with different number of prompt and non-prompt leptons can be extracted with the following relations:

$$\begin{pmatrix} N_{pp} \\ N_{pf} \\ N_{fp} \\ N_{ff} \end{pmatrix} = \begin{pmatrix} (1-p_1)(1-p_2) & (1-p_1)(1-f_2) & (1-f_1)(1-p_2) & (1-f_1)(1-f_2) \\ p_1(1-p_2) & p_1(1-f_2) & f_1(1-p_2) & f_1(1-f_2) \\ (1-p_1)p_2 & (1-p_1)f_2 & (1-f_1)p_2 & (1-f_1)f_2 \\ p_1p_2 & p_1f_2 & f_1p_2 & f_1f_2 \end{pmatrix}^{-1} \begin{pmatrix} N_{LL} \\ N_{TL} \\ N_{LT} \\ N_{TT} \end{pmatrix}, \quad (2)$$

where N_{pp}, N_{pf} (N_{fp}), and N_{ff} are the number of events with 2, 1, and 0 prompt leptons, respectively. The f_1 and f_2 are the lepton fake rates, which describe the chance of a non-prompt lepton selected as a "tight" lepton; likewise the p_1 and p_2 are the lepton prompt rates, which determine the chances of a prompt lepton selected as a "tight" lepton. The lepton fake rate and prompt rate are all measured with data. The background from events with one prompt lepton and one non-prompt lepton is estimated using N_{pf} and N_{fp}. The yield of the events with two non-prompt leptons is given by N_{ff}. The estimated background yields are in good agreement with data as summarized in Table 4.

5 Systematic uncertainties

The sources of systematic uncertainty are summarized in Table 2 for estimated backgrounds and Table 3 for simulated signal samples. The methodological uncertainty for the background estimation is determined using data control samples. Other uncertainties are applied to the simulated samples.

The uncertainty on the integrated luminosity is 2.6% [25]. The luminosity uncertainty is based on cluster counting of the silicon pixel detector. This uncertainty contributes to the expected backgrounds yields. The trigger efficiency is estimated by dividing the number of events triggered with an ensemble of MET triggers and the signal dilepton triggers, by the number of events fired with the MET trigger after requiring the number of jets to be ≥ 4. The systematic uncertainty of the trigger efficiency is contributed by the possible correlation between the MET and the dilepton triggers. The trigger systematic uncertainties on $\mu\mu$, ee, and eμ are 3.5%,4.5%, and 3.6% respectively. The lepton selection efficiencies and scale factor are determined from data-driven techniques using $Z \to \ell^+\ell^-$ events. The uncertainties for muons are determined to be 0.2% for the isolation requirement, and 0.5% for the other selection criteria. After requiring the number of jets to be ≥ 4, the scale factors for muons and electrons are varied by 0.3% and 0.1%, respectively. The uncertainty on the scale factor for lepton selection is determined to be 1% per lepton. The systematic uncertainty associated with additional pileup interactions is estimated by varying the total inelastic cross section by 5%. The uncertainties on pileup re-weighting for the irreducible backgrounds are 1.5%,0.5%, and 0.5% for $\mu\mu$, ee, and eμ. Jet energies have been corrected with dependencies on p_T and η, and the uncertainties associated with the jet energy correction factors are included as a systematic uncertainty. Furthermore, the jet energy resolution in data is worse than that in the simulation. This effect is also included as a systematic uncertainty. The background with two prompt leptons of the same charge is irreducible and is estimated with the simulated samples. The uncertainties associated with the cross sections for ttZ and ttW processes (30%) [26], and for the two and three boson processes (50%) are included as systematic uncertainties. The methodological uncertainty for the background estimation is the dominant systematic uncertainty, which is mainly contributed by the lepton fake rates and charge misidentification rate for electrons. For the fake rate, away jet p_T

variation with $\pm$ 20 GeV, S_T, number of jets, flavor difference, and statistics of control region are considered as a systematic uncertainties. The uncertainty from the fake rates in the expected number of events is less than 50%. A variation of $\pm$ 5 GeV of the Z boson mass is applied to the prompt rate. The dependence on lepton p_T, η, and the number of jets in the prompt rate is considered as a systematic uncertainty. For the charge mis-identification rate, the dependence on electron p_T, MET, and jet activity is considered. The uncertainties on the prompt rate and charge mis-identification rate are 10% and 30%, respectively. Uncertainties on the parton distribution functions are provided by the LHAPDF [27] recipe. The uncertainties caused by the limited statistics in simulated samples and the data events in the control regions are also included as a systematic uncertainty.

Systematic uncertainties (%)	$\mu\mu$	ee	μe
Integrated luminosity	1.2	0.9	1.0
Trigger efficiency	1.6	1.6	1.5
Lepton selection	0.9	0.7	0.8
Pileup events	0.7	0.2	0.2
Jet energy scale	2.6	2.3	2.6
Jet energy resolution	2.7	2.6	3.0
Background Normalization	17.9	14.5	15.1
Accuracy of control-sample method Error	26.7	30.3	30.1
Parton distribution function reweighting	2.3	1.8	1.9
Total systematic uncertainty (%)	32.5	33.9	34.0
Statistical uncertainties (%)	5.4	4.8	4.8

Table 2: The systematic uncertainties on ΔB / B for each of the $\mu\mu$, ee, and μe channels. Total systematic uncertainties are calculated by summing all systematic uncertainties in quadrature. Total 15 channels of systematic uncertainties(S_T bins for $\mu\mu$, ee, and μe channels) are separately measured.

Systematic uncertainties (%)	$\mu\mu$	ee	μe
Integrated luminosity	2.6	2.6	2.6
Trigger efficiency	3.5	4.6	3.8
Lepton selection	2.0	2.0	2.0
Pileup events	2.2	2.1	0.7
Jet energy scale	1.8	1.2	1.8
Jet energy resolution	1.6	1.5	1.5
Parton distribution function reweighting	3.0	3.0	3.0
Total systematic uncertainty (%)	6.9	7.3	6.7
Statistical uncertainties (%)	6.4	6.8	4.8

Table 3: The systematic uncertainties on $\Delta\epsilon_S$ / ϵ_S for $\mu\mu$, ee, and μe channels of simulated signal samples. For this table, the signal samples of $\mathcal{B}(b' \to tW) = 100\%$ at 600 GeV are used. Total systematic uncertainties calculated by summing all systematic uncertainties in quadrature. A total of 15 channels of systematic uncertainties (S_T bins for $\mu\mu$, ee, and μe channels) are separately measured.

6 Result

A search for pair-produced vector-like quarks of charge $-\frac{1}{3}$ in pp collisions at $\sqrt{s} = 8$ has been presented. As summarized in Table 4, there are 29, 33 and 57 events found in the $\mu\mu$, ee, and μe channels, respectively, based on a sample collected by the CMS experiment at the LHC corresponding to an integrated luminosity of 19.6 fb^{-1}. The estimated background yields are 29 ± 10, 35 ± 12, and 66 ± 22 for $\mu\mu$, ee, and μe channels, respectively. The observed data is consistent with the estimated background, and no excess has been found. Figure 2 shows the S_{T} distributions for $\mu\mu$, ee, and μe channels. Upper limits on $\mathrm{b}'\overline{\mathrm{b}}'$ pair production cross sections at 95% CL are derived, using a modified frequentist approach (CL_s [28]). The limits are calculated using fifteen bins as a log-normal distribution, given by five S_{T} bins($200 \leq S_{\mathrm{T}} < 400$, $400 \leq S_{\mathrm{T}} < 600$, $600 \leq S_{\mathrm{T}} < 800$, $800 \leq S_{\mathrm{T}} < 1200$, and $S_{\mathrm{T}} \geq 1200$) and three channels($\mu\mu$, ee, and μe). The limits on the b' masses are found to be between 464 GeV to 800 GeV at 95% confidence level for various combinations of the branching fractions of b' decaying to tW, bZ, and bH. For the most favorable scenario (with 100% $\mathrm{b}' \to \mathrm{tW}$ decay), the expected and observed limits on the b' mass are 800 GeV and 798 GeV at 95% confidence level, respectively, as shown in Figure 3. For the scenarios of $\mathcal{B}(\mathrm{b}' \to \mathrm{tW}) + \mathcal{B}(\mathrm{b}' \to \mathrm{bZ}) = 100\%$ and $\mathcal{B}(\mathrm{b}' \to \mathrm{tW}) + \mathcal{B}(\mathrm{b}' \to \mathrm{bH}) = 100\%$, the expected (observed) limits as a function of branching fractions are shown in Figure 4. The limits for any combination of branching fractions are shown in Figure 5.

Table 4: The events yield of this analysis in the signal region. Errors are a total quadratic sum of systematic uncertainty and statistical uncertainty.

$\mu\mu$	Total Events Yield	$200 \leq S_T < 400$	$400 \leq S_T < 600$	$600 \leq S_T < 800$	$800 \leq S_T < 1200$	$S_T \geq 1200$
Data	29	5	12	5	6	1
Background Estimation	29.16 ± 1.59 (stat.) ± 10.37 (sys.)	6.14 ± 0.84 (stat.) ± 2.61 (sys.)	12.50 ± 1.08 (stat.) ± 4.25 (sys.)	6.45 ± 0.67 (stat.) ± 2.03 (sys.)	3.39 ± 0.44 (stat.) ± 1.17 (sys.)	0.68 ± 0.15 (stat.) ± 0.32 (sys.)
Prompt-Prompt	13.61	0.99	4.97	4.13	2.84	0.68
Prompt-NonPrompt	15.09	5.04	7.30	2.23	0.53	0.00
NonPrompt-NonPrompt	0.46	0.11	0.24	0.08	0.03	0.00
Charge Flip	0.00	0.00	0.00	0.00	0.00	0.00
ee	Total Events Yield	$200 \leq S_T < 400$	$400 \leq S_T < 600$	$600 \leq S_T < 800$	$800 \leq S_T < 1200$	$S_T \geq 1200$
Data	33	5	19	5	4	0
Background Estimation	34.84 ± 1.68 (stat.) ± 12.05 (sys.)	5.49 ± 0.73 (stat.) ± 2.11 (sys.)	14.91 ± 1.14 (stat.) ± 5.26 (sys.)	8.67 ± 0.79 (stat.) ± 2.83 (sys.)	4.52 ± 0.56 (stat.) ± 1.43 (sys.)	1.24 ± 0.25 (stat.) ± 0.42 (sys.)
Prompt-Prompt	12.42	1.11	4.52	3.58	2.42	0.79
Prompt-NonPrompt	17.93	3.25	8.30	4.31	1.66	0.41
NonPrompt-NonPrompt	1.29	0.39	0.62	0.15	0.14	0.00
Charge Flip	3.20	0.74	1.47	0.63	0.30	0.05
μe	Total Events Yield	$200 \leq S_T < 400$	$400 \leq S_T < 600$	$600 \leq S_T < 800$	$800 \leq S_T < 1200$	$S_T \geq 1200$
Data	57	10	28	9	8	2
Background Estimation	65.55 ± 3.16 (stat.) ± 21.94 (sys.)	9.32 ± 1.37 (stat.) ± 3.46 (sys.)	29.27 ± 2.19 (stat.) ± 10.21 (sys.)	14.14 ± 1.33 (stat.) ± 4.31 (sys.)	10.77 ± 1.15 (stat.) ± 3.28 (sys.)	2.05 ± 0.46 (stat.) ± 0.67 (sys.)
Prompt-Prompt	25.41	2.03	9.13	7.14	5.86	1.25
Prompt-NonPrompt	37.62	6.58	19.10	6.55	4.62	0.77
NonPrompt-NonPrompt	0.77	0.41	0.11	0.13	0.13	0.00
Charge Flip	1.74	0.30	0.94	0.32	0.15	0.03

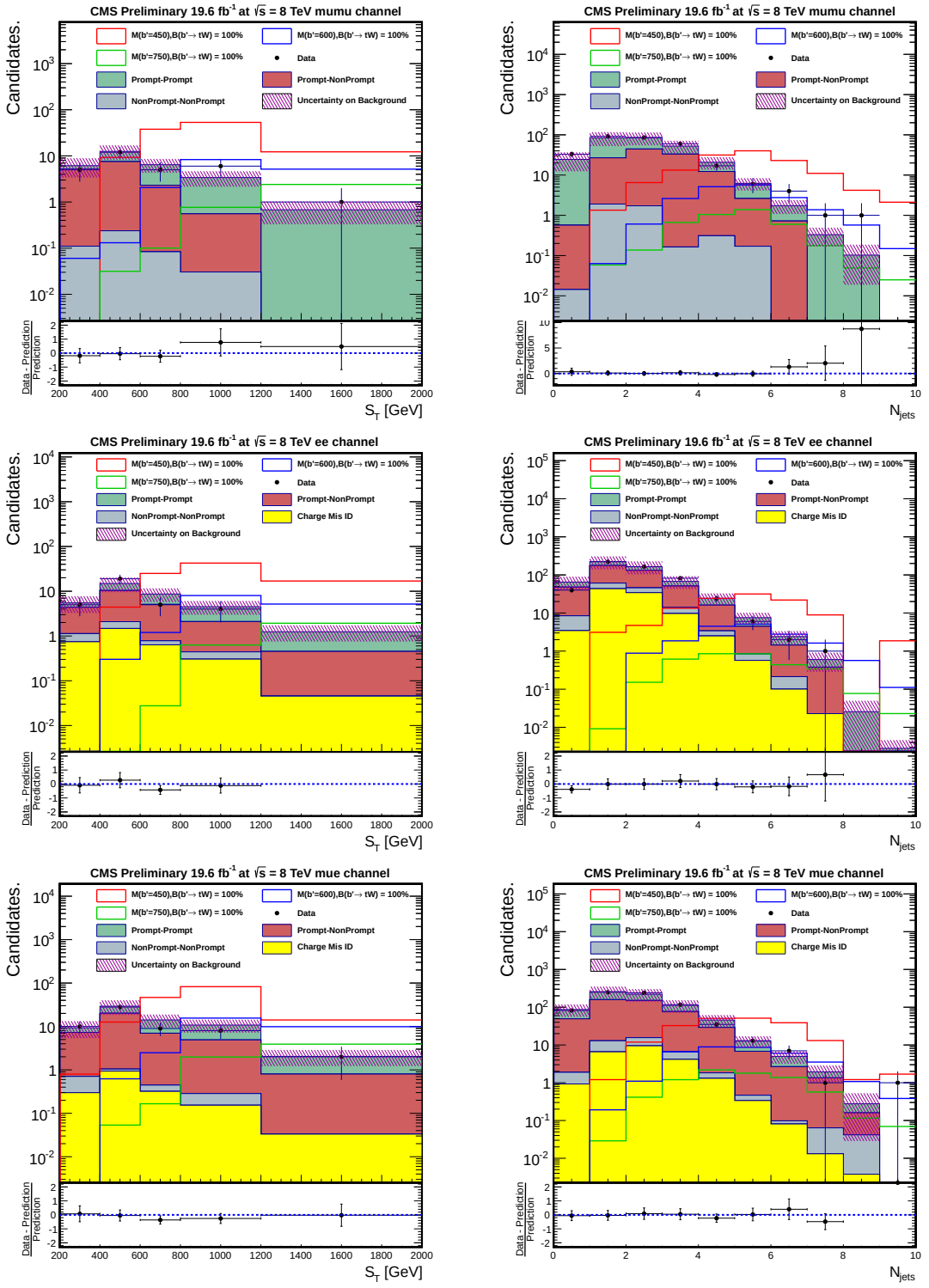

Figure 2: Full selection applied apart the requirement on the plotted variable plots of S_T with number of jets $\geq$ 4 are shown in the left and full selection applied apart the requirement on the plotted variable plots of number of jets with $S_T \geq$ 200GeV are shown in the right for the same-sign $\mu\mu$(top), ee(middle), μe(bottom) channels.

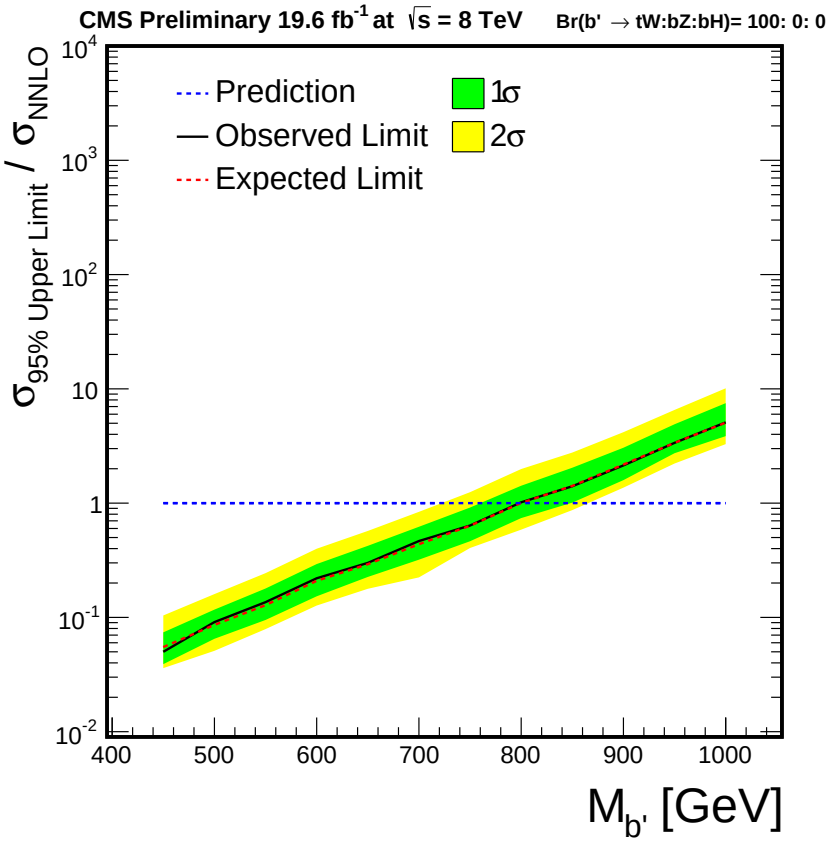

Figure 3: The exclusion limits at the 95% confidence level normalized by next-next-leading order of b′ cross sections as a function of b′ mass($M_{b'}$) assuming the branching ratio B(b′ → tW$^-$) = 100%.

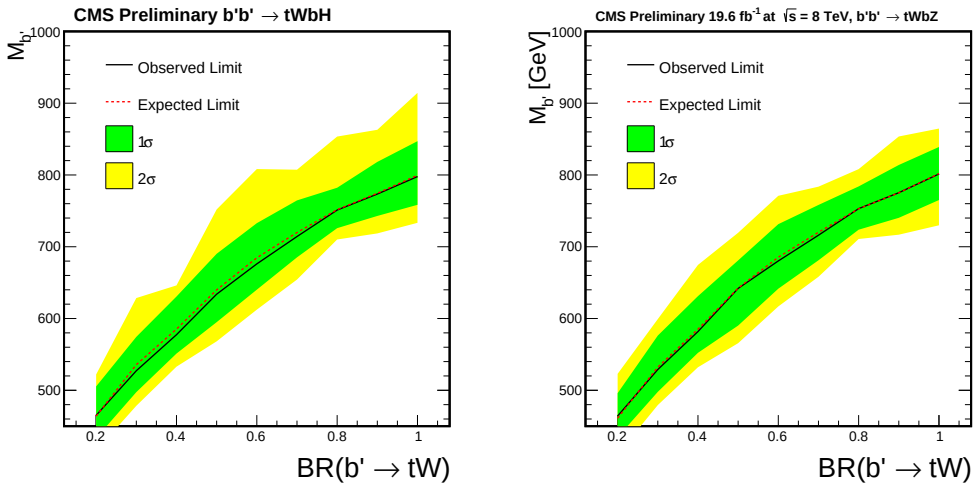

Figure 4: Plot of exclusion limit for branching ratio B(b′ → tW$^-$) + B(b′ → bH) = 100%(left) and branching ratio B(b′ → tW$^-$) + B(b′ → bZ) = 100%(right).

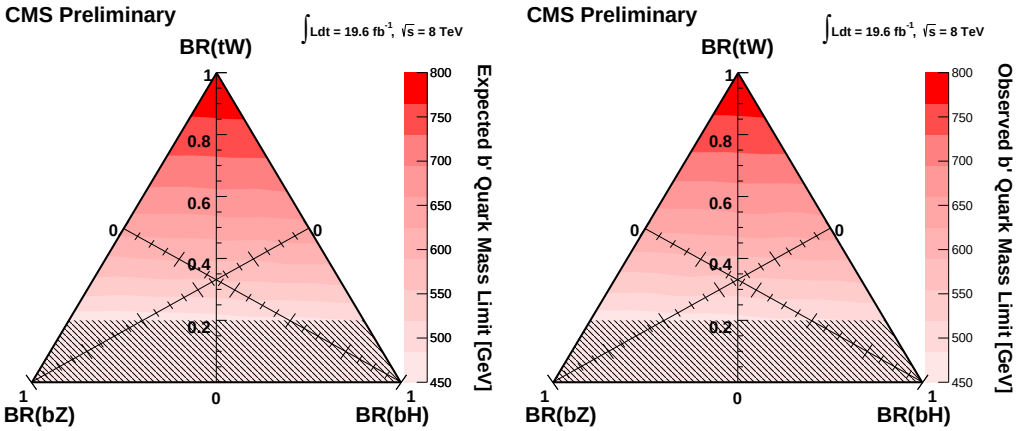

Figure 5: Plot of exclusion limit according to sixty six branching ratio combinations with an assumption of $B(b' \to tW^-) + B(b' \to bZ) + B(b' \to bH)$=100%. Expected(observed) limits are shown at each branching ratio in left(right) side. The maximum expected(observed) limit obtained is 800 GeV (798 GeV) at 95% CL, for $B(b' \to tW^-) = 100\%$. The b' mass limits for the shaded line regions are lower than 450 GeV which is the lowest mass point simulated for this analysis.

Branching ratio (%)			Expected limit (GeV)					Observed limit (GeV)
$b' \to tW$	$b' \to bZ$	$b' \to bH$	Median	-2 σ	-1 σ	+1 σ	+2 σ	
50	25	25	646	- 117	- 54	+ 48	+ 79	641
20	0	80	486	- 48	- 45	+ 38	+ 56	486
20	10	70	482	- 113	- 42	+ 36	+ 56	485
20	20	60	478	- 91	- 40	+ 37	+ 55	480
20	30	50	478	- 72	- 35	+ 39	+ 58	482
20	40	40	472	- 58	- 35	+ 33	+ 54	475
20	50	30	468	- 59	- 33	+ 31	+ 51	472
20	60	20	467	- 58	- 37	+ 37	+ 50	470
20	70	10	464	- 95	- 37	+ 31	+ 48	465
20	80	0	464	- 58	- 41	+ 31	+ 48	465
30	0	70	548	- 87	- 43	+ 39	+ 65	546
30	10	60	544	- 73	- 47	+ 38	+ 63	540
30	20	50	543	- 68	- 48	+ 39	+ 64	539
30	30	40	542	- 72	- 40	+ 37	+ 58	536
30	40	30	536	- 83	- 44	+ 34	+ 58	530
30	50	20	536	- 107	- 32	+ 36	+ 57	534
30	60	10	533	- 78	- 47	+ 33	+ 54	526
30	70	0	536	- 93	- 39	+ 38	+ 57	527
40	0	60	601	- 109	- 38	+ 33	+ 56	592
40	10	50	601	- 62	- 37	+ 28	+ 58	593
40	20	40	593	- 84	- 46	+ 37	+ 65	588
40	30	30	595	- 148	- 55	+ 41	+ 64	586
40	40	20	594	- 112	- 51	+ 40	+ 63	586
40	50	10	590	- 73	- 46	+ 38	+ 69	580
40	60	0	585	- 61	- 45	+ 34	+ 52	577
50	0	50	650	- 54	- 34	+ 29	+ 44	648
50	10	40	647	- 111	- 80	+ 48	+ 71	641
50	20	30	648	- 109	- 59	+ 45	+ 86	645
50	30	20	641	- 127	- 64	+ 45	+ 70	638
50	40	10	641	- 132	- 59	+ 45	+ 70	635
50	50	0	640	- 112	- 50	+ 45	+ 72	634
60	0	40	690	- 98	- 45	+ 43	+ 64	681
60	10	30	686	- 115	- 51	+ 41	+ 69	679
60	20	20	687	- 90	- 60	+ 45	+ 68	679
60	30	10	684	- 95	- 48	+ 42	+ 69	676
60	40	0	685	- 124	- 48	+ 44	+ 72	676
70	0	30	722	- 62	- 38	+ 38	+ 65	716
70	10	20	722	- 63	- 37	+ 38	+ 60	717
70	20	10	720	- 83	- 38	+ 35	+ 63	714
70	30	0	720	- 88	- 45	+ 35	+ 66	714
80	0	20	754	- 66	- 31	+ 27	+ 45	753
80	10	10	753	- 56	- 35	+ 26	+ 39	751
80	20	0	752	- 102	- 31	+ 26	+ 42	751
90	0	10	777	- 52	- 37	+ 34	+ 59	775
90	10	0	775	- 88	- 44	+ 32	+ 56	773
100	0	0	800	- 115	- 48	+ 41	+ 66	798

Table 5: The b' mass limits for each set of branching ratios. The maximum expected(observed) limit obtained is 800 GeV (798 GeV) at 95% CL, for $B(b' \to tW^-) = 100\%$.

References

[1] CMS Collaboration, "Observation of a new boson at a mass of 125 GeV with the CMS experiment at the LHC", *Phys. Lett. B* **716** (2012) 30–61, doi:10.1016/j.physletb.2012.08.021, arXiv:1207.7235.

[2] ATLAS Collaboration, "Observation of a new particle in the search for the Standard Model Higgs boson with the ATLAS detector at the LHC", *Phys. Lett. B* **716** (2012) 1–29, doi:10.1016/j.physletb.2012.08.020, arXiv:1207.7214.

[3] CMS Collaboration, "Combined results of searches for the standard model Higgs boson in pp collisions at $\sqrt{s} = 7$ TeV", *Phys. Lett. B* **710** (2012) 26–48, doi:10.1016/j.physletb.2012.02.064, arXiv:1202.1488.

[4] M. Schmaltz, "Physics beyond the standard model (Theory): Introducing the Little Higgs", *Nuclear Physics B - Proceedings Supplements* **117** (2003), no. 0, 40 – 49, doi:http://dx.doi.org/10.1016/S0920-5632(03)01409-9. 31st International Conferences on High Energy Physics.

[5] D. Marzocca, M. Serone, and J. Shu, "General Composite Higgs Models", *JHEP* **1208** (2012) 013, doi:10.1007/JHEP08(2012)013, arXiv:1205.0770.

[6] N. ArkaniHamed, S. Dimopoulos, and G. Dvali, "The hierarchy problem and new dimensions at a millimeter", *Physics Letters B* **429** (1998), no. 34, 263 – 272, doi:http://dx.doi.org/10.1016/S0370-2693(98)00466-3.

[7] J. Aguilar-Saavedra, R. Benbrik, S. Heinemeyer, and M. Perez-Victoria, "A handbook of vector-like quarks: mixing and single production", *Phys. Rev. D* **88** (2013) 094010, doi:10.1103/PhysRevD.88.094010, arXiv:1306.0572.

[8] CMS Collaboration, "Inclusive search for a vector-like T quark by CMS", Technical Report CMS-PAS-B2G-12-015, CERN, Geneva, 2013.

[9] ATLAS Collaboration, "Search for pair production of heavy top-like quarks decaying to a high-p_{T} W boson and a b quark in the lepton plus jets final state in pp collisions at $\sqrt{s} = 8$ TeV with the ATLAS detector", Technical Report ATLAS-CONF-2013-060, CERN, Geneva, Jun, 2013.

[10] ATLAS Collaboration, "Search for pair production of new heavy quarks that decay to a **Z** boson and a third generation quark in **pp** collisions at $\sqrt{\mathbf{s}} = \mathbf{8}$ TeV with the ATLAS detector", Technical Report ATLAS-CONF-2013-056, CERN, Geneva, Jun, 2013.

[11] ATLAS Collaboration, "Search for anomalous production of events with same-sign dileptons and b jets in 14.3 fb^{-1} of pp collisions at $\sqrt{s} = 8$ TeV with the ATLAS detector", Technical Report ATLAS-CONF-2013-051, CERN, Geneva, May, 2013. Not published in the proceedings.

[12] ATLAS Collaboration, "Search for heavy top-like quarks decaying to a Higgs boson and a top quark in the lepton plus jets final state in pp collisions at $\sqrt{s} = 8$ TeV with the ATLAS detector", Technical Report ATLAS-CONF-2013-018, CERN, Geneva, Mar, 2013.

[13] CMS Collaboration, "Search for heavy bottom-like quarks in 4.9 inverse femtobarns of pp collisions at $\sqrt{s} = 7$ TeV", *JHEP* **1205** (2012) 123, doi:10.1007/JHEP05(2012)123, arXiv:1204.1088.

[14] CMS Collaboration, "The CMS experiment at the CERN LHC", *JINST* **03** (2008) S08004, doi:10.1088/1748-0221/3/08/S08004.

[15] CMS Collaboration, "Particle-Flow Event Reconstruction in CMS and Performance for Jets, Taus, and MET", Technical Report CMS-PAS-PFT-09-001, CERN, 2009. Geneva, Apr, 2009.

[16] CMS Collaboration, "Electron reconstruction and identification at sqrt(s) = 7 TeV", Technical Report CMS-PAS-EGM-10-004, CERN, Geneva, 2010.

[17] CMS Collaboration, "Tau identification in CMS", Technical Report CMS-PAS-TAU-11-001, CERN, Geneva, 2011.

[18] M. Cacciari, G. P. Salam, and G. Soyez, "The Anti-k_t jet clustering algorithm", *JHEP* **0804** (2008) 063, doi:10.1088/1126-6708/2008/04/063, arXiv:0802.1189.

[19] M. Cacciari, G. P. Salam, and G. Soyez, "FastJet user manual", *Eur. Phys. J. C* **72** (2012) 1896, arXiv:1111.6097.

[20] CMS Collaboration, "Determination of Jet Energy Calibration and Transverse Momentum Resolution in CMS", *JINST* **6** (2011) P11002, doi:10.1088/1748-0221/6/11/P11002, arXiv:1107.4277.

[21] F. Maltoni and T. Stelzer, "MadEvent: Automatic event generation with MadGraph", *JHEP* **0302** (2003) 027, doi:10.1088/1126-6708/2003/02/027, arXiv:hep-ph/0208156.

[22] M. Czakon and A. Mitov, "Top++: A Program for the Calculation of the Top-Pair Cross-Section at Hadron Colliders", arXiv:1112.5675.

[23] GEANT4 Collaboration, "GEANT4: A Simulation toolkit", *Nucl. Instrum. Meth. A* **506** (2003) 250–303, doi:10.1016/S0168-9002(03)01368-8.

[24] T. Sjostrand, S. Mrenna, and P. Z. Skands, "A Brief Introduction to PYTHIA 8.1", *Comput.Phys.Commun.* **178** (2008) 852–867, doi:10.1016/j.cpc.2008.01.036., arXiv:hep-ph.

[25] CMS Collaboration, "CMS Luminosity Based on Pixel Cluster Counting - Summer 2013 Update", Technical Report CMS-PAS-LUM-13-001, CERN, Geneva, 2013.

[26] J. M. Campbell and R. K. Ellis, "$t\bar{t}W^{+-}$ production and decay at NLO", *JHEP* **1207** (2012) 052, doi:10.1007/JHEP07(2012)052, arXiv:1204.5678.

[27] "LHAPDF : The Les Houches Accord PDF Interface : http://lhapdf.hepforge.org/",.

[28] A. L. Read, "Presentation of search results: the CL s technique", *Journal of Physics G: Nuclear and Particle Physics* **28** (2002), no. 10, 2693.